Materials Science & Engineering C 108 (2020) 110420

Contents lists available at ScienceDirect

Materials Science & Engineering C

journal homepage: www.elsevier.com/locate/msec

2D Graphene oxide (GO) doped *p-n* type $BiOI/Bi_2WO_6$ as a novel composite for photodegradation of bisphenol A (BPA) in aqueous solutions under UV-vis irradiation

Zhu Mengting[a,1], Tonni Agustiono Kurniawan[a,b,1,*], You Yanping[a], Ram Avtar[c], Mohd Hafiz Dzarfan Othman[d]

[a] Key Laboratory of the Coastal and Wetland Ecosystems (Xiamen University), Ministry of Education, College of Ecology and the Environment, Xiamen University, Xiamen 361102, Fujian, China
[b] China-ASEAN College of Marine Sciences, Xiamen University Malaysia, Sepang, Selangor Darul Ehsan 43900, Malaysia
[c] Faculty of Environmental Earth Science, Hokkaido University, Sapporo 060-0810, Japan
[d] Advanced Membrane Technology Research Centre (AMTEC), School of Chemical and Energy Engineering, Universiti Teknologi Malaysia, Skudai, 81310, Johor, Malaysia

ARTICLE INFO

Keywords:
BPA degradation
Carbon-based materials
Heterojunction
Hybrid photocatalysts

ABSTRACT

Bisphenol A (BPA) is a refractory pollutant presents in water body that possesses serious threats to living organisms. To deal with it, we investigate and evaluate the effectiveness of $GO@BiOI/Bi_2WO_6$ composite as a novel photocatalyst for BPA removal from aqueous solutions under UV–vis irradiation. To enhance its removal for BPA, the surface of $BiOI/Bi_2WO_6$ is modified with graphene oxide (GO). This composite is named as 'GO@BiOI/Bi_2WO_6'. Changes in its physico-chemical properties after surface modification with GO are characterized by XRD, FTIR, FESEM-EDS, XPS, PL, and BET methods. Optimized conditions of BPA degradation by the composite are determined under identical conditions. Photodegradation pathways of BPA and its removal mechanisms by the same composite are presented. It is obvious that the $GO@BiOI/Bi_2WO_6$ has demonstrated its potential as a promising photocatalyst for BPA removal under UV–vis irradiation. About 81% of BPA removal is attained by the $GO@BiOI/Bi_2WO_6$ under optimized conditions (10 mg/L of BPA, 0.5 g/L of dose, pH 7 and 5 h of reaction time). The oxidation by-products of BPA degradation include *p*-hydroquinone or 4-(1-hydroxy-1-methyl-ethyl)-phenol. In spite of its performance, the treated effluents are still unable to meet the maximum discharge limit of < 1 mg/L set by national legislation. Therefore, subsequent biological processes are essential to maximize its biodegradation in the wastewater samples before their discharge into waterbody.

1. Introduction

BPA (Fig. S1), an endocrine disrupting compound (EDCs), is widely used for making plastic products such as water bottles. Under acidic or basic conditions, the BPA is easily leached out from BPA-based products when its ester bonds linkage are hydrolyzed [1]. Due to their wide use, human exposure to the BPA is unavoidable. So far, its presence in human body has been detected in urine [2]. Although the dose of its exposure is quite low, BPA still can cause adverse health effects [3].

In spite of being hydrophobic, the BPA is often detected in aquatic environment such as landfill leachate [4,5]. Although the pollutant is present in trace quantity, recently its effluent discharge standards in wastewater have been regulated. Japan and the US set the BPA effluent limit of < 2.5 mg/L and 0.5 mg/L, respectively, while China set 1 mg/L as its maximum discharge limit.

Over the past decades, BPA contamination in the environment has been tackled using various approaches. Fig. S2 reported that the total number of BPA-related publications has increased by 600% from 1995 to date, while the total articles of water pollution due to the BPA alone has grown by 550% up to 4397 publications over the same period. By 2019, over 31,769 BPA-related articles have been cumulatively recorded in the Thomson Reuter's Web of Science, with 62% of them having been published over the past decade (2009–2019).

So far, various technologies have been tested to remove BPA from wastewater like adsorption [6], reverse osmosis [7], advanced oxidation processes (AOP) [8–10], photodegradation [11]. Due to its eco-

* Corresponding author at: Key Laboratory of the Coastal and Wetland Ecosystems (Xiamen University), Ministry of Education, College of Ecology and the Environment, Xiamen University, Xiamen 361102, Fujian, China.
E-mail address: tonni@xmu.edu.cn (T.A. Kurniawan).
[1] The first and second authors equally contribute to this article and mutually share the first authorship.

https://doi.org/10.1016/j.msec.2019.110420
Received 30 July 2019; Received in revised form 8 October 2019; Accepted 10 November 2019
Available online 13 November 2019
0928-4931/

friendly operations, photodegradation has been extensively used to remove refractory pollutants such as xenobiotic compounds in aqueous solutions [11].

When a photocatalyst absorbs visible light for generating charge carriers, photodegradation reactions occur on its active surface through the formation of ·OH, which rapidly breakdown target pollutants into CO_2, H_2O and smaller oxidation by-products [12]. However, the drawback of this technology is its high recombination rate of photogenerated electron-hole pairs (e^-, h^+) caused by low quantum yields [13]. To address this bottleneck, new photocatalysts with unique physico-chemical properties need to be tailored specifically on their surface with carbon-based materials like GO [14].

Recently, bismuth-containing photocatalysts (like Bi_2CrO_6, Bi_2WO_6, Bi_2O_3, $BiVO_4$, BiOI) have gained popularity due to their superiority. They have not only an ideal band gap of layered structure for electron migration between conduction band (c_b) and valence band (v_b) as well as strong response to visible-light, but also a rapid mobility of photogenerated charge carriers [15].

Among the Bi-based photocatalysts, both BiOI and Bi_2WO_6 are popular due to their efficient photocatalytic activities [16]. The Bi_2WO_6 has a band gap of 2.8 eV, while the BiOI has a shorter band gap (1.8 eV) [17] that enables the latter to rapidly generate electrons and holes under visible light irradiation. A preliminary study reported that a BiOI/Bi_2WO_6 exhibited higher photocatalytic activities than did individual BiOI and/or Bi_2WO_6 during photodegradation of Brilliant Red [18]. However, the short band gap of the photocatalyst led to a high recombination of its electron-hole pairs that inhibit its photocatalytic activity [19,20]. To mitigate the impacts caused by this limitation, the Bi-containing photocatalyst needs to be impregnated with another material that has unique capability of reducing the recombination rate of its hole-electron pairs and capturing photogenerated electrons.

Recently, GO has become popular due to its unique physico-chemical and electronic properties. It has a high surface area and strong mechanical properties that could be used to enhance light absorption intensity and light absorption range of a semiconductor [21–23]. Its surface consists of oxygenated functional groups such as −OH, C—O and =COO- that could be involved in separating photogenerated carriers of a semiconductor and prolonging the lifetime of its electron-hole pairs.

So far none has reported the applicability of the GO doped with BiOI/Bi_2WO_6 for BPA removal in contaminated water. In order to fill this research gap, we investigate the effectiveness of GO@BiOI/Bi_2WO_6 composite as a novel photocatalyst for BPA removal from aqueous solutions under UV-vis irradiation. To enhance its removal for target pollutant, GO that has high surface area and excellent mechanical strength was applied to modify the surface of BiOI/Bi_2WO_6. With respect to its novelty, it is the first attempt to use a hydrothermal method in synthesizing 'GO@BiOI/Bi_2WO_6'. This new photocatalyst has advantages including simple operation, rapid fabrication and high yield.

Changes in its physico-chemical properties after surface modification with GO were analyzed by an X-ray diffractometer (XRD), Fourier transformation infrared (FTIR), field emission scanning electron microscope-energy dispersive spectroscopy (FESEM-EDS), X-ray photoelectron spectros-copy (XPS), photoluminescence spectra (PL spectra), and Brunauer-Emmett-Teller (BET) methods. Optimum conditions of BPA degradation by the GO@BiOI/Bi_2WO_6 composite were determined under identical conditions. The photodegradation pathways of BPA and its removal mechanisms by the same composite under UV-Vis irradiation were also elaborated.

2. Materials and methods

2.1. Materials

Both $BiNO_3{\cdot}5H_2O$ and $Na_2WO_6{\cdot}2H_2O$ were obtained from Xilong Scientific (China). Ethylene glycol (EG) was supplied by Sinopharm Chemical (China), while BPA (Table S1) was provided by Aladdin Industrial Co. (China). One g of BPA was dissolved in 1 L of C_2H_5OH as a stock solution, while its working solutions were freshly prepared. Natural graphite powder, provided by Macklin Technology (China), was used to prepare GO using a modified Hummers method [24].

2.2. Methods

2.2.1. Synthesis of GO@BiOI/Bi_2WO_6 composite

The GO@BiOI/Bi_2WO_6 was prepared by a solvothermal method [16]. After dissolving both $BiNO_3{\cdot}5H_2O$ and KI into EG solution, the mixture was mechanically stirred for 30 min at ambient temperature. Simultaneously, $Na_2WO_6{\cdot}2H_2O$ was dissolved into the same EG solution by adding it dropwise into the mixture, and then kept it stirring for 3 h until a homogenous mixture was formed. Subsequently, the mixture was transferred to a hydrothermal reactor. After heating it at 453 K for 24 h and cooling it down at ambient temperature overnight, the product was washed with ultrapure water, dried at 353 K in an oven and grounded. This was called as 'BiOI/Bi_2WO_6 composite' (w/w = 1:1).

To synthesize GO@BiOI/Bi_2WO_6, both one g of the BiOI/Bi_2WO_6 composite and 0.10 g of GO were dispersed into 50 mL of deionized water and then ultrasounded for 1.5 h. After they were completely mixed, the mixture was transferred into a hydrothermal reactor and heated at 433 K in an oven for 4 h. After cooling it down at ambient temperature, the mixture was centrifuged at 6000 rpm for 20 min. The resulting solid was repeatedly washed with ultrapure water and dried at 353 K. After grinding it into powder, the GO@BiOI/Bi_2WO_6 was collected and stored in a desiccator for further use. For its comparison to the GO@BiOI/Bi_2WO_6, both the Bi_2WO_6 and the BiOI/Bi_2WO_6 composite were also freshly prepared under identical conditions using the same solvothermal method.

2.2.2. Characterization of photocatalyst

The resulting GO@BiOI/Bi_2WO_6 was characterized by an X-ray diffractometer (Rigaku, Japan) using Cu *Kα* radiation that operated at 40 kV and 30 mA at 10°/min from 5° to 80° [25,26]. Their BET specific surface areas were tested using a N_2 adsorption-desorption isotherm analysis at 77 *K* (ASAP2020, US). The FTIR spectra of the same photocatalyst were recorded on an IS50 (Thermo, US) in the range of 4000–400 cm^{-1} with a resolution of 0.2 cm^{-1}. Changes in its morphology were observed using a FESEM-EDS (Sigma, Germany). The elemental composition of the samples was identified by an X-ray photoelectron spectroscopy (Thermo Escalab, UK). The photoluminescence (PL) spectrum was analyzed using a Fluorescence Spectrophotometer (model F-7000, Hitachi, Japan).

2.2.3. Photodegradation experiments

About 0.7 g of the GO@BiOI/Bi_2WO_6 was mixed with 300 mL of BPA with its concentration ranging from 5 to 25 mg/L. After 1 h of dark reaction, there was no BPA removal by the photocatalyst in the solution, indicating that an equilibrium between the former and the latter was established [27,28]. The system was placed in an airtight photoreactor under Xenon illumination (500 W) and continuously stirred to undergo reactions. The scheme of the photodegradation reactor is presented in Fig. S3.

2.2.4. Chemical analysis of BPA

After treatment, 5 mL of the suspensions were collected periodically for chemical analysis of the remaining BPA concentrations. The pollutant's absorbance intensity was determined using a UV–vis spectrophotometer (model UV-1800, Shanghai, China). The maximum absorption wavelength of BPA was at 278 nm [29]. The removal efficiency of BPA η(%) was calculated based on the Eq. (1):

$$\eta(\%) = [(c_0 - c_e)/c_0] \times 100\% \quad (1)$$

where c_0 and c_e represents the initial and the final concentrations of

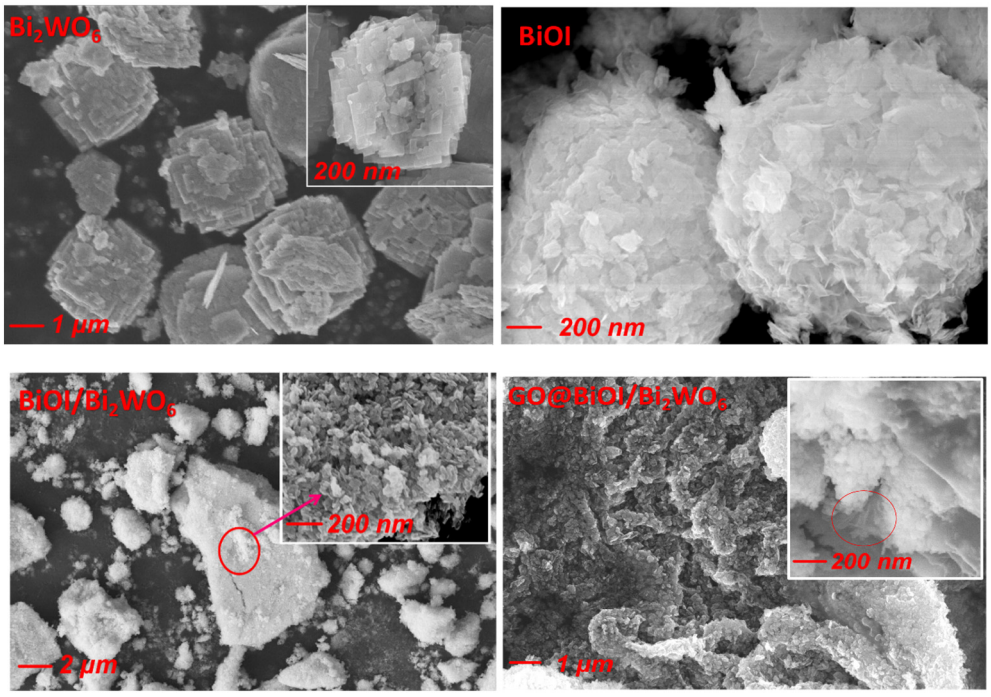

Fig. 1. SEM analyses of various photocatalysts.

BPA after UV-Vis irradiation, respectively.

2.3. Statistical analysis

Under identical conditions, all of the photodegradation experiments were carried out in duplicate. The obtained data were presented as an average value of the replication with their variation coefficients of < 5%. All statistical analyses were conducted using SPSS 25.0 Windows version. The differences were statistically significant when $p \leq 0.05$.

3. Results and discussions

3.1. Characterization of composites

3.1.1. SEM

Changes in the morphology of the composite after the introduction of GO on its surface were examined by using SEM. The SEM images of the individual Bi_2WO_6, BiOI, BiOI/Bi_2WO_6 hybrid and GO@BiOI/Bi_2WO_6 composites are presented in Fig. 1.

Fig. 1 shows a nanoplate-like structure of the Bi_2WO_6 sample. This reveals that the nanoplates were stacked together through a layer-by-layer manner to form disc-shaped architectures. This finding was in agreement with those reported by Zhang et al. [30] and Wang et al. [31], who also found that the synthesized Bi_2WO_6 had microdisk morphologies.

The BiOI consisted of many nanosheets that appeared like a blooming flower with a smooth surface [32–34]. Although the Bi_2WO_6 and BiOI particles were mixed and uniformly distributed during the synthesis of the BiOI/Bi_2WO_6 composite, its morphology changed since the BiOI occupied the surface of the nanosheet that covered the Bi_2WO_6 particles. The short distance of the two semiconductors promoted an efficient separation of photogenerated electron-hole (e^-, h^+) pairs, thus improving their photocatalytic activities [35].

Based on its SEM analyses (Fig. 1), the wrinkled structure of the GO@BiOI/Bi_2WO_6 composite appeared on the GO surface because the spherical BiOI particles and the Bi_2WO_6 nanoplates were also deposited on the same GO surface. The results confirm those of previous study undertaken by Hojamberdiev et al. [16], who found that the hierarchical structures of the Bi_2WO_6 and BiOI particles could be found on the *r*GO surface. Their structure might contribute to the reactive site of the composite during photodegradation of the BPA.

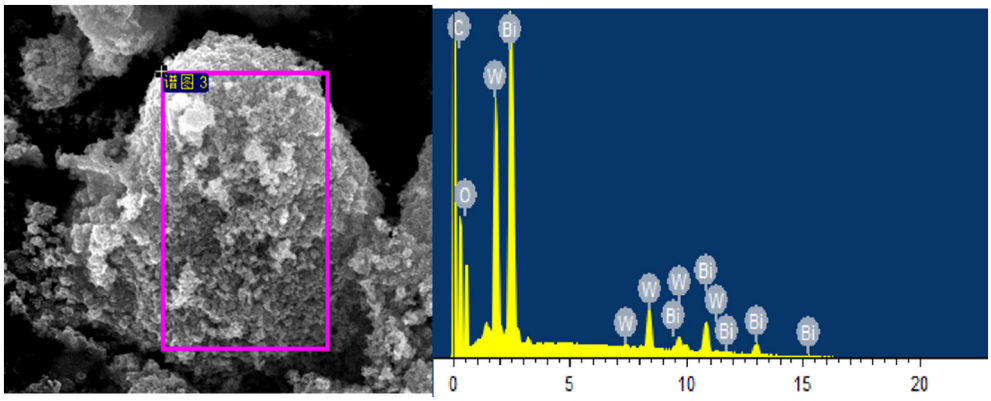

Fig. 2. EDS microanalyses of GO@BiOI/Bi_2WO_6 composite.

Fig. 2 presents the elemental composition of the GO@BiOI/Bi_2WO_6 composite using EDS analyses. The result indicated the presence of C, O, Bi, W, with their composition of 23, 14, 19 and 44% (w/w), respectively. The C content on the surface of the sample confirmed the existence of GO, indicating that the GO was successfully doped into the BiOI/Bi_2WO_6 composite [36]. The Iodine composition in the composite was negligible due to the low content of the sample. Alzamly et al. [32] found that the amount of iodine was directly related to the loading of BiOI into the composite.

3.1.2. XPS

The elemental compositions of the GO@BiOI/Bi_2WO_6 composite were further characterized by an XPS (Fig. S4). All elemental signals of the GO@BiOI/Bi_2WO_6 composite were detected in the XPS spectra and their results were compatible and consistent with those of EDS analyses.

Fig. S4-a illustrates the spectra of the GO@BiOI/Bi_2WO_6 composite and demonstrates the presence of C, Bi, O, W, and I elements in the sample. The peak at 159.3 eV in Fig. 4S-b corresponded to the Bi 4f of the same sample (Fig. S4-b), while the binding energies of W 4f and I 3d, respectively, are 35.7 and 619.2 eV, corresponding to the W^{6+} [37,38] and/or the I^- [39]. The findings were in agreement with the results reported earlier by Sriwichai et al. [36], who found the presence of Bi^{3+} with its corresponding binding energy.

3.1.3. XRD

To understand their respective structural differences in terms of crystallinity, the crystaline structures of all types of the photocatalysts (Bi_2WO_6, BiOI, BiOI/Bi_2WO_6 and GO@BiOI/Bi_2WO_6 composite) were analyzed by using XRD tests (Fig. 3).

Fig. 3 presents that all of the photocatalysts have strong and sharp diffraction peaks, which indicates their high level of crystallinity. Some diffraction peaks could be indexed to the orthorhombic phase of the Bi_2WO_6 (PDF card 26-1044, JCPDS), while the other peaks were suitable to the tetragonal phase of the BiOI (PDF card 10-0445, JCPDS). This suggests that the synthesis of the individual Bi_2WO_6 and the BiOI formed the crystallinity of the composite.

With respect to the Bi_2WO_6/BiOI composite, Fig. 3 shows that its diffraction peaks matched well with the orthorhombic phase of the Bi_2WO_6. However, there were neither separate peaks of the BiOI nor impurities found in the Bi_2WO_6/BiOI composite. This reveals that the BiOI might be completely integrated into the Bi_2WO_6/BiOI composite during its synthesis. This finding is in agreement with that of previous study carried out by Wang et al. [40] found that the diffraction intensity of the BiOI was relatively low, while the strong diffraction of the Bi_2WO_6 peaks led to the disappearance of the characteristic peaks of their composite.

In addition, the broad diffraction peaks of the GO were not present in the XRD patterns of the composite. Theoretically, the XRD spectra of

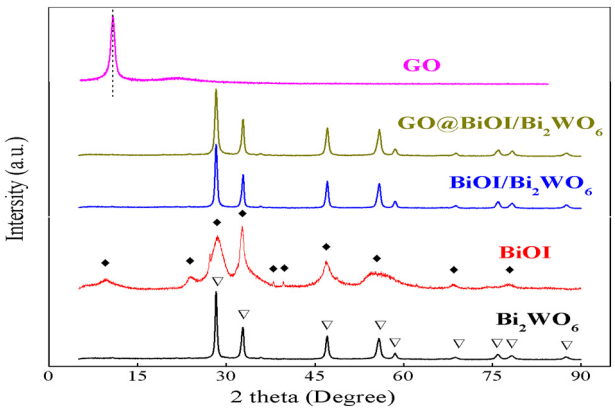

Fig. 3. XRD patterns of various photocatalysts.

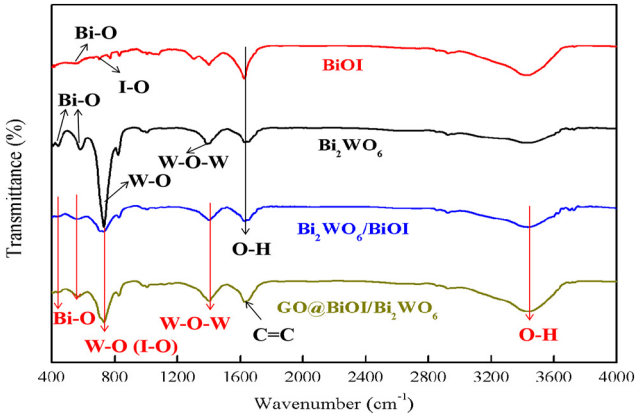

Fig. 4. FTIR spectra of various photocatalysts.

the GO sheets in sharp diffraction peaks should be present at 10° [41,42]. This could be due to the presence of the high-intensity diffraction peaks of the Bi_2WO_6/BiOI composite that suppressed GO's peaks [16].

3.1.4. FTIR

To understand the chemical structures of all the composites synthesized, their FTIR spectra were examined and analyzed. Their results are presented in Fig. 4.

Fig. 4 depicts that both the BiOI/Bi_2WO_6 and the GO@BiOI/Bi_2WO_6 composite possessed absorption bands ranging from 400–1000 cm^{-1}, attributed to the Bi−O and the W−O stretching, respectively [43,44]. The characteristic absorption peaks at 580 cm^{-1} and 1385 cm^{-1} are assigned to the stretching vibration of the W−O and the W-O-W, respectively, while the peaks at 485 cm^{-1} and at 725 cm^{-1} belong to the Bi−O stretching vibration [45,46]. The peak at 1620 cm^{-1} corresponds to the C=C stretching of the GO, while the broad band at 3420 cm^{-1} is ascribed to the O−H stretching vibration of the water molecules in the samples [24,47,48]. It is also observed from Fig. 4 that the peak width of the GO@BiOI/Bi_2WO_6 composite became broader as the bands (I−O, W−O) of each starting compound (BiOI, Bi_2WO_6) appear to have an almost overlapping position.

Overall, the results of the FTIR analyses suggest that the GO@BiOI/Bi_2WO_6 composite have functional groups that include BiOI, Bi_2WO_6 as well as GO. This indicates that its synthesis process was complete. Hence, the composite could be tested as a photocatalyst for promoting BPA removal.

3.1.5. Photoluminescence spectra (PL)

PL emission intensity results from the recombination of free charge carriers and this corresponds with photocatalytic performances [49,50]. Therefore, this method was applied to determine the photoinduced charge separation and migration efficiencies of photocatalysts.

Fig. S5 presents the photoluminescence (PL) spectra of the pure Bi_2WO_6, the BiOI/Bi_2WO_6 and the GO@BiOI/Bi_2WO_6 samples. As depicted in Fig. S5, the PL spectrum of the Bi_2WO_6 suggests a high photoinduced charge recombination rate due to its intrinsic properties. The PL intensity of the BiOI/Bi_2WO_6 composite was lower than that of the pure Bi_2WO_6. This result indicates that the conjunction of BiOI and Bi_2WO_6 promotes an efficient separation of the photoinduced charge carriers and prolongs its life, thus improving their photocatalytic activities [51].

In addition, the PL spectra of the GO@BiOI/Bi_2WO_6 had the lowest emission peak intensity. This suggests that the synthesis of the composite effectively promoted the photogenerated charge separation and migration of charge carriers during photodegradation reaction. Xu et al. [51] reported that semiconductors with lower PL intensities tended to exhibit higher photocatalytic activities due to their lower charge

recombination rate.

3.1.6. BET

Surface areas of composites contribute to their removal performance during photodegradation of target pollutants. Therefore, it is necessary to analyze their porous properties and surface areas by using N_2 physisorption measurement [16]. Fig. S6 represents the typical N_2 adsorption-desorption isotherms of pure Bi_2WO_6, individual BiOI, BiOI/Bi_2WO_6 and GO@BiOI/Bi_2WO_6 composite. Their specific surface areas calculated by the BET method (S_{BET}) are also presented in the same figure.

Changes in the N_2 adsorption-desorption isotherms of all the composites show identical type II isotherm according to the IUPAC's classification. This testifies an adsorption of N_2 on a non-porous or microporous adsorbent with strong adsorbate-adsorbent interactions [52].

While the average pore size of the GO@BiOI/Bi_2WO_6 was 28.62 nm, the calculated S_{BET} values of individual Bi_2WO_6, BiOI, BiOI/Bi_2WO_6 and/or GO@BiOI/Bi_2WO_6 composite are 11.52, 51.59, 23.81 and 22.79 $m^2 \cdot g^{-1}$, respectively (Table S2). The S_{BET} of GO@BiOI/Bi_2WO_6 composite was lower than that of the BiOI because the Bi_2WO_6 particles loaded on the composite had a small specific surface area that affected its S_{BET} by reducing its porosity. Therefore, the pore size of the samples contributes to the change in the composite's BET surface areas [53,54]. The bigger the pore size of the composite is, the larger its BET surface area is. The results also confirmed the findings reported earlier by Hojamberdiev et al. [16], who found that the S_{BET} values of the GO@BiOI/Bi_2WO_6 composite usually ranged between 20 and 25 $m^2 \cdot g^{-1}$.

3.2. Photocatalytic activity

Previous work, in agreement with our findings, indicates that the dark reaction lasts between 0.5–1 h [27,28]. After the adsorbent and the adsorbate have sufficient physico-chemical interactions in the solution, an equilibrium state between the amount of the BPA adsorbed and that of the BPA still present in the solution is established. After 1 h, there was no longer BPA removal by the adsorbent. As a result, the final concentration of BPA was the adsorbate's equilibrium concentration and 1 h was the optimum time after which there was no longer BPA removal.

3.2.1. Comparison of BPA photodegradation by various composites

Fig. 5 shows the degradation performance of BPA using individual Bi_2WO_6, BiOI/Bi_2WO_6 and GO@BiOI/Bi_2WO_6 composite under UV–vis irradiation, respectively.

Under the same conditions (BPA concentration: 10 mg/L, 0.5 g/L of dose, pH 9), during the 5 h of UV–vis irradiation, the Bi_2WO_6 and the BiOI/Bi_2WO_6 composite exhibited a relatively low BPA removal of 47% and 50%, respectively. This could be due to less UV light utilization and low quantum efficiency of the two photocatalysts. After introducing the GO into the surface of the BiOI/Bi_2WO_6 composite, the BPA removal by the GO@BiOI/Bi_2WO_6 composite has substantially improved up to 73% under identical conditions. Therefore, this composite was selected for subsequent studies.

The improvement of BPA removal by the GO@BiOI/Bi_2WO_6 composite could be due to the synergistic effects between the surface of GO and the BiOI/Bi_2WO_6 composite through combined adsorption and photocatalysis. In this composite, each material has its own function. The BiOI/ Bi_2WO_6 composite is capable of enhancing its quantum efficiency and improving light harvesting efficiency for promoting rapid oxidative reactions of BPA through the formation of •OH, while the GO provides specific surface areas that act as active sites for adsorption purposes [55,56].

3.2.2. Effect of initial pH on BPA removal by GO@BiO/Bi_2WO_6

In water treatment applications, pH affects the extent of target pollutant's removal by the surface of a photocatalyst because its active sites are dependent on the concentration of H^+ or OH^- in aqueous solutions [57]. After the selected photocatalyst was determined based on the results in Fig. 6, a series of studies was conducted to determine the optimum pH for BPA removal by the composite by varying the solution pH from 3 to 11.

As depicted in Fig. 6, after 1 h of reaction, with its initial concentration of 10 mg/L, about 0.5 g/L the GO@BiOI/Bi_2WO_6 composite attained a maximum BPA removal of 80% at pH 7. This optimum pH was used for subsequent photodegradation studies.

It is important to note that a weak acidic pH range from pH 5 to pH 7 was more effective for BPA removal by the composite than an alkaline pH. This could be attributed to the surface charge density of the composite and the electrostatic charge of the BPA anions at varying pH values. At acidic pH ranges, a weak acid like BPA with p$Ka \approx 9.60$ is dissociated at pH $>$ pKa [58] and present in its molecular form, while the composite has negative charges due to the GO. As a result, attractive columbic forces occurred between the negative charge of the photocatalyst and the protonated BPA.

On the other hand, in basic conditions (pH $>$ 8), the BPA molecules are deprotonated (pH $>$ pH_{pzc}) firstly at pH 8 and secondly at pH 9, respectively, where BPA^{2-} and $HBPA^-$ represent major anionic species [59].

$$BPA^{2-} + H^+ \rightarrow HBPA^- \; pKa = 10.42 \quad (2)$$

$$BPA^{2-} + 2H^+ \rightarrow H_2BPA \; pKa = 20.05 \quad (3)$$

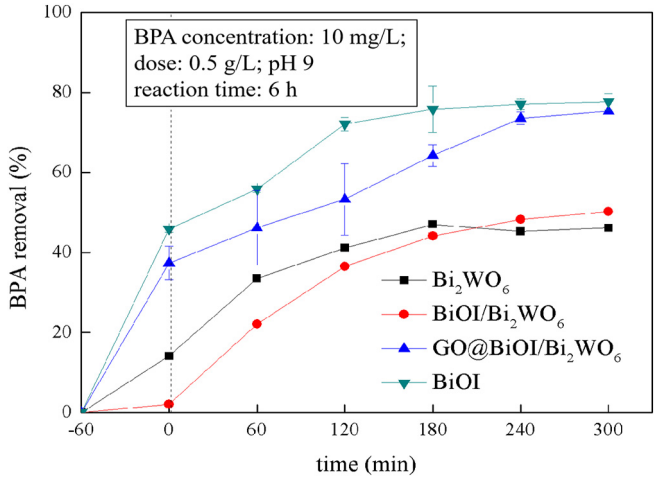

Fig. 5. Performances of various photocatalysts for BPA photodegradation.

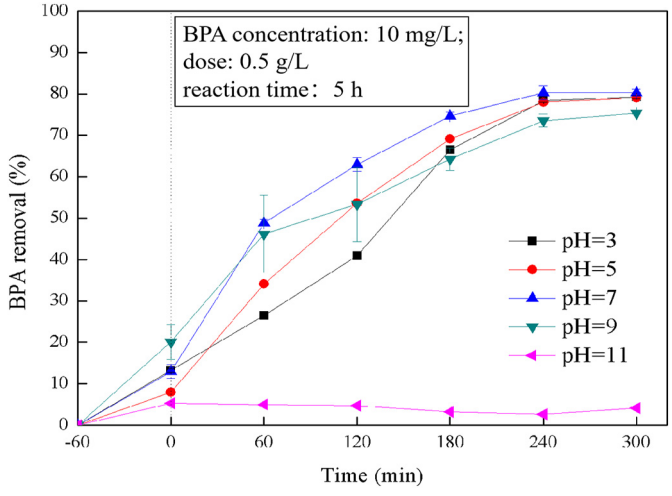

Fig. 6. Effects of pH on BPA degradation by GO@BiOI/Bi_2WO_6.

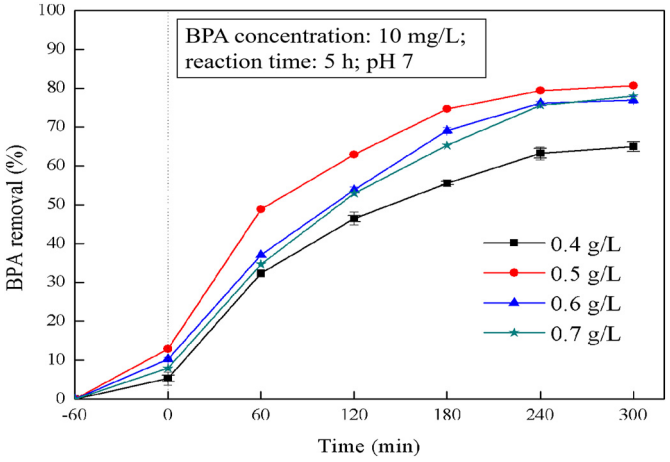

Fig. 7. Effects of dose on BPA degradation by GO@BiOI/Bi_2WO_6.

Under alkaline environment, the BPA molecules are ionized to mono- or divalent anion after deprotonation. Consequently, this results in electrostatic repulsions between the increasingly ionized adsorbate molecules with their negative charge and the negatively charged surface of the photocatalyst, leading to a lower BPA removal by the composite during photodegradation [60].

3.2.3. Effect of photocatalyst's dose on BPA degradation by GO@BiOI/Bi_2WO_6

To investigate the effects of dose on BPA degradation by the photocatalyst, the dose of the GO@BiOI/Bi_2WO_6 composite was varied from 0.4 to 0.7 g/L under optimized conditions (BPA concentration: 10 mg/L, pH 7.0, and 5 h of reaction time). Fig. 7 shows that 0.5 g/L was the optimum dose of the composite that attained the highest BPA degradation of 81% under the same conditions.

The BPA removal by the photocatalyst was enhanced from 65% to 81% with its increasing dose from 0.4 to 0.5 g/L. An optimum dose of the composite would maximize not only the surface area of the photocatalyst, but also the number of its active sites for producing •OH during UV–vis irradiation [55]. However, an excessive dose of the composite could be counter-productive to the BPA removal because of the increasing mass transfer of resistance and light shielding effects that inhibit the photodegradation rate under UV-Vis irradiation [61]. Therefore, it is important to use 0.5 g/L as the optimum dose to attain a maximum BPA removal by the composite.

3.2.4. Photodegradation mechanisms of BPA by GO@BiOI/Bi_2WO_6

To understand its removal mechanisms, Fig. 8 illustrates the BPA photodegradation by the GO@BiOI/Bi_2WO_6 composite. Under UV–vis irradiation, electrons (e^-) and holes (h^+) are generated on the surface of GO@BiOI/Bi_2WO_6 (Eqs. (4)–(5)). The electrons are trapped on its surface that subsequently separate the charge carriers [62,63].

After both the BiOI and the Bi_2WO_6 absorb photons individually, electrons excite from valence band (v_b) to conduction band (c_b), resulting in the generation of photogenerated holes (h^+) in the valence band (v_b) and photogenerated electrons (e^-) in the conductive band (c_b). Due to the internal electric field [25], the h^+ in the v_b of the Bi_2WO_6 migrates to the v_b of the BiOI, while the e^- in the c_b of the BiOI move to the corresponding c_b of the Bi_2WO_6.

Since the Bi_2WO_6 has a band gap of 1.8 eV, while the BiOI exhibits a longer band gap of 2.78 eV, Li et al. [64] and Moniz et al. [65] found that the electron migration in the composite during the BPA photodegradation was attributed to the *p-n* heterojunction formed by the *p*-type BiOI and the *n*-type Bi_2WO_6 that also promote separation of (e^-, h^+) pairs. The h^+ might be ensnared by surface-adsorbed OH^- to generate •OH, while the e^- might be entrapped by the adsorbed O_2 on the surface of the composite to generate $\bullet O_2^-$ that subsequently reacts with the target pollutant.

The BPA molecules, adsorbed on the surface of the photocatalyst, are then oxidized due to photogenerated holes (h^+) and subsequently generate oxidation by-products. The electrons (e^-) react with O_2 on the surface of the composite to produce •OH (Eqs. (6)–(9)). Part of the BPA molecules are oxidized by $\bullet O_2^-$, while the other was degraded by •OH into smaller and more biodegradable oxidation by-products, CO_2 and H_2O (Eq. (10)).

The overall mechanisms of BPA removal by the GO@BiOI/Bi_2WO_6 are proposed as follow:

$$\text{GO@BiOI/Bi}_2\text{WO}_6\ (h\nu) \rightarrow \text{GO@BiOI/Bi}_2\text{WO}_6\ (e^- + h^+) \quad (4)$$

$$\text{GO@BiOI/Bi}_2\text{WO}_6\ (e^- + h^+) \rightarrow \text{GO@BiOI/Bi}_2\text{WO}_6\ (e^-) + \text{GO@BiOI/Bi}_2\text{WO}_6\ (h^+) \quad (5)$$

$$H_2O \rightarrow H^+ + OH^- \quad (6)$$

$$\text{GO@BiOI/Bi}_2\text{WO}_6\ (e^-) + O_2 \rightarrow \bullet O_2^- \quad (7)$$

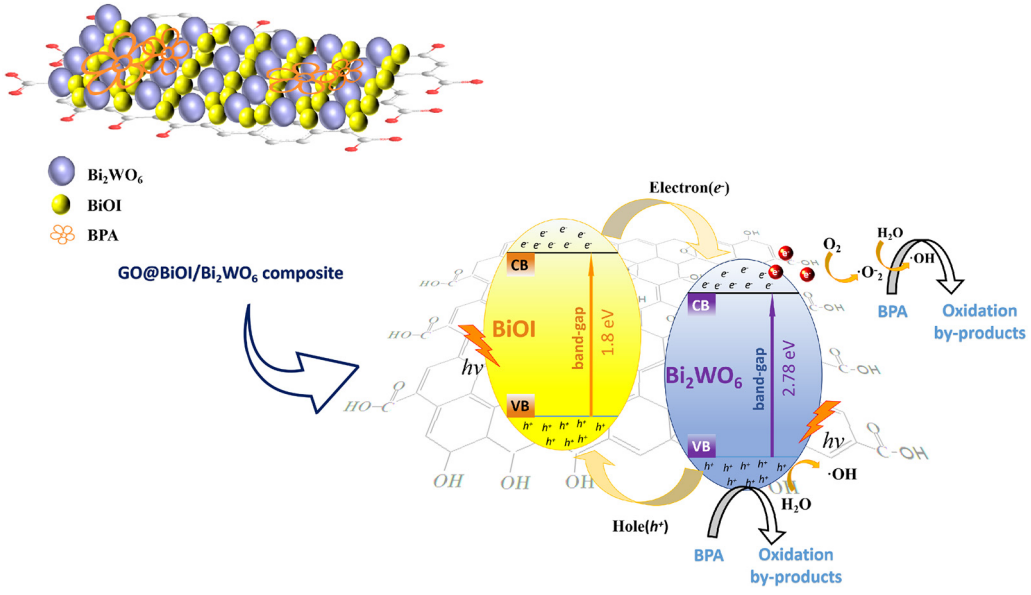

Fig. 8. Removal mechanisms of BPA using GO@BiOI/Bi_2WO_6 composite.

Table 1
Comparison of removal performance by different photocatalysts.

Target pollutant	Hybrid photocatalyst	Concentration (mg/L)	Dose (g/L)	pH	Reaction time (min)	Removal efficiency (%)	References
BPA	GO@BiOI/Bi_2WO_6	10	0.5	7	300	81%	Present study
	Ag_3PO_4/$LaCo_{0.5}Bi_{0.5}O_3$	10	0.5	NA[e]	40	87%	[74]
	*r*GO/silica/zirconia	10	0.4	7	90	87%	[75]
	AgI/BiOI	10	25	NA[e]	120	92%	[76]
	BiOI/BiOCl	20	1	7	60	97%	[73]
	Ag/BiOI/*r*GO	0.01	1	NA[e]	80	100%	[72]
4-CP[a]	GO/CDots[d]/BiOI	20	1	NA[e]	180	98%	[77]
Cr(VI)	rGO/BiOI/ZnO	10	0.7	3	180	92%	[78]
MO[b]	TiO_2/WO_3/GO	20	0.02	7	120	74%	[29]
MB[c]	$BaTiO_3$/GO	5	0.5	9	180	95%	[54]

Remark: 4-CP[a]: 4-chlorophenol MO[b]: Methyl orange MB[c]: Methyl blue CDots[d]: carbon nanodots NA[e]: not available.

$$\bullet O_2^- + H^+ \rightarrow \bullet HO_2 \quad (8)$$

$$GO@BiOI/Bi_2WO_6\,(h^+) + OH^- \rightarrow \bullet OH \quad (9)$$

$$BPA + (h^+, \bullet O_2^-, \bullet OH) \rightarrow \text{Oxidation by} - \text{products} \rightarrow CO_2 + H_2O \quad (10)$$

Due to its large surface area, the GO not only contributes to the migration of charge carriers, but also prolongs the lifetime of photogenerated carriers, leading to the formation of free radicals for photocatalytic degradations of BPA [66]. It is important to determine oxidation by-products including hydroquinone or 4-(1-hydroxy-1-methyl-ethyl)-phenol during BPA removal, as previous studies reported [67–71].

Fig. S7 presents the photodegradation pathways of BPA by the GO@BiOI/Bi_2WO_6 composite under UV–vis irradiation. After BPA is indiscriminately attacked by the •OH, this reaction generates intermediate products such as succinic, fumaric and oxalic acids before being mineralized into CO_2 and H_2O. Their free electrons may be involved in the transfer of 4-isopropyl group or benzene ring of the BPA, resulting in the formation of phenol, hydroquinone and/or 4-(1-hydroxy-1-methyl-ethyl)-phenol, respectively, as confirmed by Sharma et al. [71] and Molkenthin et al. [70], respectively.

3.3. Comparison of various BPA degradation studies

To justify its feasibility as an effective photocatalyst for removal of refractory pollutants, the degradation performance of BPA by the GO@BiOI/Bi_2WO_6 composite is evaluated and compared to those of previous studies. To compare their performance fairly, comparative studies are presented with respect to pollutant's concentration (mg/L), photocatalyst's dose (g/L), optimum pH, reaction time (min) and removal efficiency (%).

Table 1 presents a summary of composites such as Ag/BiOI/*r*GO, Ag_3PO_4/ $LaCo_{0.5}Bi_{0.5}O_3$, BiOI/BiOCl, AgI/BiOI and *r*GO/silica/zirconia used as photocatalysts for BPA removal. About 1 g/L of Ag/BiOI/*r*GO could attain a complete removal of BPA with its concentration of 0.01 mg/L after 80 min [72], while 97% of BPA degradation with its concentration of 20 mg/L was achieved using BiOI/BiOCl after 60 min [73]. Under the same BPA concentration of 10 mg/L, the [13] BPA removal by Ag_3PO_4/$LaCo_{0.5}Bi_{0.5}O_3$, *r*GO/ silica/zirconia, and/or AgI/BiOI photocatalysts were 87%, 87%, and 92%, respectively [74-76].

Under optimized conditions of 10 mg/L of BPA concentration, 0.5 g/L of dose and pH 7, 81% of BPA removal was achieved. Since its treated effluents still could not meet the maximum discharge standard of < 1 mg/L set by China's regulation, further activated sludge are necessary to complete the biodegradation of the remaining oxidation by-products of BPA in the effluent samples.

4. Conclusions

This work has demonstrated that the BiOI/Bi_2WO_6 composite is promising and applicable for BPA removal only after it was doped with the GO. About 81% of BPA removal was attained by the GO@BiOI/Bi_2WO_6 photocatalyst under optimum conditions (10 mg/L of BPA concentration, 0.5 g/L of dose, pH 7 and 5 h of reaction time). The oxidation by-products of BPA include *p*-hydroquinone or 4-(1-hydroxy-1-methyl-ethyl)-phenol. In spite of the composite's promising performance, its treated effluents were still unable to meet the maximum discharge standard of lower than 1 mg/L set by local legislation. Therefore, subsequent biological processes are required to complement the biodegradation of BPA.

Acknowledgements

The authors are grateful to the TYAN (The World Academy of Sciences' Young Affiliates Network) for providing them with the Collaborative Grant Award No. FR 3240304540.

Appendix A. Supplementary data

Supplementary data to this article can be found online at https://doi.org/10.1016/j.msec.2019.110420.

References

[1] J. Sajiki, J. Yonekubo, Leaching of bisphenol A (BPA) from polycarbonate plastic to water containing amino acids and its degradation by radical oxygen species, Chemosphere 55 (2004) 861–867.
[2] M. Guida, J. Troisi, C. Ciccone, G. Granozio, C. Cosimato, A.D. Sardo, C. Ferrara, M. Guida, C. Nappi, F. Zullo, C. Di Carlo, Bisphenol A and congenital developmental defects in humans, Mutat. Res-Fund Mol. M. 774 (2015) 33–39.
[3] J.G. Hengstler, H. Foth, T. Gebel, P.J. Kramer, W. Lilienblum, H. Schweinfurth, W. Volkel, K.M. Wollin, U. Gundert-Remy, Critical evaluation of key evidence on the human health hazards of exposure to bisphenol A, Crit. Rev. Toxicol. 41 (2011) 263–291.
[4] T.A. Kurniawan, G. Chan, W.H. Lo, Radicals-catalyzed oxidation for degradation of recalcitrant compounds from landfill leachate, Chem. Eng. J. 125 (2006) 35–57.
[5] T.A. Kurniawan, W. LO, G. Chan, Physico-chemical treatments for removal of recalcitrant contaminants from leachate, J. Hazard. Maters 129 (2006) 80–100.
[6] L. Yanyan, T.A. Kurniawan, A. Albadarin, G. Walker, Enhanced removal of acetaminophen from synthetic wastewater using multi-walled carbon nanotubes (MWCNT) chemically modified with NaOH, HNO_3/H_2SO_4, ozone, and/or chitosan, J. Mol. Liq. 251 (2018) 369–377.
[7] G. Chan, C. Jie, T.A. Kurniawan, C. Fu, Removal of non-biodegradable compounds from stabilized leachate using VSEPRO membrane filtration, Desalination 202 (2007) 310–317.
[8] M. Vilve, S. Vilhunen, M. Vepsäläinen, T.A. Kurniawan, N. Lehtonen, H. Isomäki, M. Sillanpaa, Degradation of 1,2-dichloroethane from contaminated water laden with ion-exchange resin using Fenton's oxidation, Environ. Sci. Pollut. Res. 17 (2010) 875–884.
[9] D. Fu, Y. Huang, X. Zhang, T.A. Kurniawan, T. Ouyang, Uncovering potentials of integrated TiO_2(B) nanosheets and H_2O_2 for removal of tetracycline from aqueous solution, J. Mol. Liq. 248 (2017) 112–130.
[10] P.L. Wang, X. Zhou, Y.G. Zhang, L.P. Yang, K.K. Zhi, L.L. Wang, L.T. Zhang, X.F. Guo, Unveiling the mechanism of electron transfer facilitated regeneration of active Fe^{2+} by nano-dispersed iron/graphene catalyst for phenol removal, RSC Adv. 7 (2017) 26983–26991.
[11] T.A. Kurniawan, Y.Y. Lin, O. Tong, A.B. Albadarin, G. Walker, $BaTiO_3$/TiO_2 composite-assisted photocatalytic degradation for removal of acetaminophen from synthetic wastewater under UV-vis irradiation, Maters. Sci. Semicond. Proc. 73 (2018) 42–50.

[12] N.M. Mohtora, H.D. Othman, S.A. Bakarb, T.A. Kurniawan, H. Dzinuna, M.N.A.M. Norrdina, Synthesis of nanostructured titanium dioxide layer onto kaolin hollow fibre membrane via hydro-thermal method for decolorisation of reactive black 5, Chemosphere 208 (2018) 595–605.

[13] A. Jilani, H.D. Othman, O. Ansari, R. Kumar, I.U. Khan, A. Wahab, A. Alshahrie, M.A. Barakat, T.A. Kurniawan, Visible light active nickel oxide@graphene oxide nanocomposite thin films: optical, dielectric, XPS surface chemical state and enhanced photocatalytic investigation, J. Maters. Sci. 53 (2018) 15034–15050.

[14] P.L. Wang, X. Zhou, Y.G. Zhang, L.L. Wang, K.K. Zhi, Y.F. Jiang, Synthesis and application of magnetic reduced graphene oxide composites for the removal of bisphenol A in aqueous solution-a mechanistic study, RSC Adv. 6 (2016) 102348–102358.

[15] M. Sillanpaa, T.A. Kurniawan, W.H. Lo, Degradation of chelating agents in aqueous solution using advanced oxidation process (AOP), Chemosphere 83 (2011) 1443–1460.

[16] M. Hojamberdiev, Z.C. Kadirova, R.V. Goncalves, K. Yubuta, N. Matsushita, K. Teshima, M. Hasegawa, K. Okada, Reduced graphene oxide-modified Bi_2WO_6/BiOI composite for the effective photocatalytic removal of organic pollutants and molecular modeling of adsorption, J. Mol. Liq. 268 (2018) 715–727.

[17] X.C. Meng, Z.S. Zhang, New insight into BiOX (X = Cl, Br, and I) hierarchical microspheres in photocatalysis, Maters. Lett. 225 (2018) 152–156.

[18] H.Q. Li, Y.M. Cui, W.S. Hong, High photocatalytic performance of BiOI/Bi_2WO_6 toward toluene and reactive brilliant red, Appl. Surf. Sci. 264 (2013) 581–588.

[19] Y.H. Liang, X. Wang, W.J. An, Y. Li, J.S. Hu, W.Q. Cui, Ag-C_3N_4@ppy-rGO 3D structure hydrogel for efficient photocatalysis, Appl. Surf. Sci. 466 (2019) 666–672.

[20] F.Y. Chen, W.J. An, L. Liu, Y.H. Liang, W.Q. Cui, Highly efficient removal of bisphenol A by a three-dimensional graphene hydrogel-AgBr@rGO exhibiting adsorption/photocatalysis synergy, Appl. Catal. B-Environ. 217 (2017) 65–80.

[21] D. Fu, T.A. Kurniawan, H. Li, L. Wang, Z. Chen, H. Wang, W. Li, Y. Wang, Q. Li, Applicability of HDPC-supported Cu nanoparticles composite synthesized from unused waste digestate for octocrylene degradation in aqueous solutions, Chem. Eng. J. 355 (2019) 650–660.

[22] Y. Zhang, W.Q. Cui, W.J. An, L. Liu, Y.H. Liang, Y.F. Zhu, Combination of photoelectrocatalysis and adsorption for removal of bisphenol A over TiO_2-graphene hydrogel with 3D network structure, Appl. Catal. B-Environ. 221 (2018) 36–46.

[23] L. Yanyan, T.A. Kurniawan, Z. Yi, A. Albadarin, G. Walker, Enhanced photocatalytic degradation of acetaminophen from wastewater using WO3/TiO2/SiO2 composite under UV-VIS irradiation, J. Mol. Liq. 243 (2017) 761–770.

[24] X.F. Wang, K.A.S. Fernando, V. Watson, C.E. Bunker, Synthesis of graphene oxide from graphite using modified Hummer's method and related studies, Process. Eng. (2012) 244.

[25] T.A. Kurniawan, W. LO, M. Sillanpaa, Treatment of contaminated water laden with 4-chlorophenol using coconut shell waste-based activated carbon modified with chemical agents, Sep. Sci. Technol. 46 (2011) 460–472.

[26] T. Huuha, T.A. Kurniawan, M. Sillanpa, Removal of silicon from pulping whitewater using integrated treatment of chemical precipitation & evaporation, Chem. Eng. J. 158 (2010) 584–592.

[27] R.Y. Wu, H.B. Song, N. Luo, Y. Sheng, G.J. Ji, Microwave-assisted preparation and enhanced photocatalytic activity of Bi_2WO_6/BiOI heterojunction for organic pollutants degradation under visible-light irradiation, Solid State Sci. 87 (2019) 101–109.

[28] X.Y. Kong, W.Q. Lee, A.R. Mohamed, S.P. Chai, Effective steering of charge flow through synergistic inducing oxygen vacancy defects and p-n heterojunctions in 2D/2D surface-engineered Bi_2WO_6/BiOI cascade: towards superior photocatalytic CO_2 reduction activity, Chem. Eng. J. 372 (2019) 1183–1193.

[29] X.Y. Hao, M. Li, L. Zhang, K.K. Wang, C.G. Liu, Photocatalyst TiO_2/WO_3/GO nanocomposite with high efficient photocatalytic performance for BPA degradation under visible light and solar light illumination, J. Ind. Eng. Chem. 55 (2017) 140–148.

[30] D.D. Zhang, F.Y. Dai, P. Zhang, Z.H. An, Y.P. Zhao, L. Chen, The photodegradation of methylene blue in water with PVDF/GO/ZnO composite membrane, Maters. Sci. Eng. C-Maters. 96 (2019) 684–692.

[31] X.J. Wang, L.L. Chang, J.R. Wang, N.N. Song, H.L. Liu, X.L. Wan, Facile hydrothermal synthesis of Bi_2WO_6 microdiscs with enhanced photocatalytic activity, Appl. Surf. Sci. 270 (2013) 685–689.

[32] A. Alzamly, M. Bakiro, S.H. Ahmed, S.M. Sallabi, R.A. Al Ajeil, S.A. Alawadhi, H.A. Selem, S.S.M. Al Meshayei, A. Khaleel, N. Al-Shamsi, N. Saleh, Construction of BiOF/BiOI nanocomposites with tunable band gaps as efficient visible-light photocatalysts, J. Photochem. Photobiol. A 375 (2019) 30–39.

[33] L. Wang, D.B.A. Yan, L. Lyu, C. Hu, N. Jiang, L.L. Zhang, Notable light-free catalytic activity for pollutant destruction over flower-like BiOI microspheres by a dual-reaction-center Fenton-like process, J. Coll. Int. Sci. 527 (2018) 251–259.

[34] L. Zeng, F. Zhe, Y. Wang, Q.L. Zhang, X.Y. Zhao, X. Hu, Y. Wu, Y.M. He, Preparation of interstitial carbon doped BiOI for enhanced performance in photocatalytic nitrogen fixation and methyl orange degradation, J. Coll. Int. Sci. 539 (2019) 563–574.

[35] L. Pan, S.B. Wang, J.W. Xie, L. Wang, X.W. Zhang, J.J. Zou, Constructing TiO_2 p-n homojunction for photoelectrochemical and photocatalytic hydrogen generation, Nano Energy 28 (2016) 296–303.

[36] S. Sriwichai, H. Ranwongsa, K. Wetchakun, S. Phanichphant, N. Wetchakun, Effect of iron loading on the photocatalytic performance of Bi_2WO_6 photocatalyst, Superlattice. Microst. 76 (2014) 362–375.

[37] Y.K. Zou, Y.X. Gong, B.Z. Lin, N.P. Mellott, Photodegradation of methylene blue in the visible spectrum: An efficient W^{6+} ion doped anatase titania photocatalyst via a solvothermal method, Vacuum 126 (2016) 63–69.

[38] J.S. Lu, Y.J. Wang, F. Liu, L. Zhang, S.N. Chai, Fabrication of a direct Z-scheme type WO_3/Ag_3PO_4 composite photocatalyst with enhanced visible-light photocatalytic performances, Appl. Surf. Sci. 393 (2017) 180–190.

[39] X.D. Su, J.J. Yang, X. Yu, Y. Zhu, Y.M. Zhang, In situ grown hierarchical 50%BiOCl/BiOI hollow flowerlike microspheres on reduced graphene oxide nanosheets for enhanced visible-light photocatalytic degradation of rhodamine B, Appl. Surf. Sci. 433 (2018) 502–512.

[40] Y.Q. Wang, S. Jiang, F. Liu, C.C. Zhao, D.F. Zhao, X.F. Li, Study on preparation and toluene removal of BiOI/Bi_2WO_6/ACF photocatalyst, Appl. Surf. Sci. 488 (2019) 161–169, https://doi.org/10.1016/j.apsusc.2019.05.228.

[41] T.A. Kurniawan, W. LO, E. Repo, M. Sillanpaa, Removal of 4-chlorophenol from contaminated water using coconut shell waste pretreated with chemical agents, J. Chem. Technol. Biotechnol. 85 (2010) 1616–1627.

[42] F.T. Johra, J.W. Lee, W.G. Jung, Facile and safe graphene preparation on solution based platform, J. Ind. Eng. Chem. 20 (2014) 2883–2887.

[43] C.S. Guo, Y. He, P. Du, X. Zhao, J.P. Lv, W. Meng, Y. Zhang, J. Xu, Novel magnetically recoverable BiOBr/iron oxides heterojunction with enhanced visible light-driven photocatalytic activity, Appl. Surf. Sci. 320 (2014) 383–390.

[44] J.G. Yu, J.F. Xiong, B. Cheng, Y. Yu, J.B. Wang, Hydrothermal preparation and visible-light photocatalytic activity of Bi_2WO_6 powders, J. Solid State Chem. 178 (2005) 1968–1972.

[45] Z. Liu, X.X. Xu, J.Z. Fang, X.M. Zhu, J.H. Chu, B.J. Li, Microemulsion synthesis, characterization of bismuth oxyiodine/titanium dioxide hybrid nanoparticles with outstanding photocatalytic performance under visible light irradiation, Appl. Surf. Sci. 258 (2012) 3771–3778.

[46] I. Ardelean, S. Cora, D. Rusu, EPR and FT-IR spectroscopic studies of Bi_2O_3-B_2O_3-CuO glasses, Physica B 403 (2008) 3682–3685.

[47] S.Y. Dong, X.H. Ding, T. Guo, X.P. Yue, X. Han, J.H. Sun, Self-assembled hollow sphere shaped Bi_2WO_6/RGO composites for efficient sunlight-driven photocatalytic degradation of organic pollutants, Chem. Eng. J. 316 (2017) 778–789.

[48] D. Jamwal, G. Kaur, P. Raizada, P. Singh, D. Pathak, P. Thakur, Twin-tail surfactant peculiarity in superficial fabrication of semiconductor quantum dots: toward structural, optical, and electrical features, J. Phys. Chem. C 119 (2015) 5062–5073.

[49] J.C. Yu, J.G. Yu, W.K. Ho, Z.T. Jiang, L.Z. Zhang, Effects of F^- doping on the photocatalytic activity and microstructures of nanocrystalline TiO_2 powders, Chem. Maters. 14 (2002) 3808–3816.

[50] S. Kuriakose, V. Choudhary, B. Satpati, S. Mohapatra, Enhanced photocatalytic activity of Ag-ZnO hybrid plasmonic nanostructures prepared by a facile wet chemical method, Beilstein J. Nanotech. 5 (2014) 639–650.

[51] Q.C. Xu, D.V. Wellia, Y.H. Ng, R. Amal, T.T.Y. Tan, Synthesis of porous and visible-light absorbing Bi_2WO_6/TiO_2 heterojunction films with improved photoelectrochemical and photocatalytic performances, J. Phys. Chem. C 115 (2011) 7419–7428.

[52] M. Thommes, K. Kaneko, A.V. Neimark, J.P. Olivier, F. Rodriguez-Reinoso, J. Rouquerol, K.S.W. Sing, Physisorption of gases, with special reference to the evaluation of surface area and pore size distribution (IUPAC Technical Report), Pure Appl. Chem. 87 (2015) 1051–1069.

[53] Y.Y. Gao, X.P. Pu, D.F. Zhang, G.Q. Ding, X. Shao, J. Ma, Combustion synthesis of graphene oxide-TiO_2 hybrid materials for photodegradation of methyl orange, Carbon 50 (2012) 4093–4101.

[54] M.T. Zhu, T.A. Kurniawan, F. Song, T. Ouyang, M.H.D. Othman, M. Rezakazemi, S. Shirazian, Applicability of $BaTiO_3$/graphene oxide (GO) composite for enhanced photodegradation of methylene blue (MB) in synthetic wastewater under UV–vis irradiation, Environ. Pollut. 255 (2019) 113182.

[55] H.H. Chun, W.K. Jo, Adsorption and photocatalysis of 2-ethyl-1-hexanol over graphene oxide-TiO_2 hybrids post-treated under various thermal conditions, Appl. Catal. B-Environ. 180 (2016) 740–750.

[56] J.C. Lyu, Z. Hu, Z.L. Li, M. Ge, Removal of tetracycline by BiOBr microspheres with oxygen vacancies: combination of adsorption and photocatalysis, J. Phys. Chem. Solids 129 (2019) 61–70.

[57] A.B. Albadarin, S. Solomon, T.A. Kurniawan, C. Mangwandi, G. Walker, Single, simultaneous and consecutive biosorption of Cr(VI) and orange II onto chemically modified masau stones, J. Environ. Manage. 204 (2017) 365–374.

[58] P.V.L. Reddy, K.H. Kim, B. Kavitha, V. Kumar, N. Raza, S. Kalagara, Photocatalytic degradation of bisphenol A in aqueous media: a review, J. Environ. Manag. 213 (2018) 189–205.

[59] N. Hirayama, W. Umehara, Novel separation of inorganic anions using a charged complex ion-exchanger, Anal. Chim. Acta 334 (1996) 1–4.

[60] H.J. Zheng, K.J. Zhu, Q.L. Wu, J.S. Liu, J.H. Qiu, Preparation and characterization of monodispersed $BaTiO_3$ nanocrystals by sol-hydrothemal method, J. Cryst. Growth 363 (2013) 300–307.

[61] K. Mehrotra, G.S. Yablonsky, A.K. Ray, Macro kinetic studies for photocatalytic degradation of benzoic acid in immobilized systems, Chemosphere 60 (2005) 1427–1436.

[62] J.X. Low, S.W. Cao, J.G. Yu, S. Wageh, Two-dimensional layered composite photocatalysts, Chem. Commun. 50 (2014) 10768–10777.

[63] Z.Q. Wu, L.M. Wang, Graphene oxide (GO) doping hexagonal flower-like ZnO as potential enhancer of photocatalytic ability, Maters. Lett. 234 (2019) 287–290.

[64] X. Li, J.G. Yu, J.X. Low, Y.P. Fang, J. Xiao, X.B. Chen, Engineering heterogeneous semiconductors for solar water splitting, J. Maters. Chem. A 3 (2015) 2485–2534.

[65] S.J.A. Moniz, S.A. Shevlin, D.J. Martin, Z.X. Guo, J.W. Tang, Visible-light driven heterojunction photocatalysts for water splitting - a critical review, Energy Environ. Sci. 8 (2015) 731–759.

[66] R.A. He, S.W. Cao, D.P. Guo, B. Cheng, S. Wageh, A.A. Al-Ghamdi, J.G. Yu, 3D BiOI-GO composite with enhanced photocatalytic performance for phenol degradation under visible-light, Ceram. Int. 41 (2015) 3511–3517.

[67] J.X. Liu, F.X. Xie, R. Li, T. Li, Z.H. Jia, Y.F. Wang, Y.W. Wang, X.C. Zhang, C.M. Fan,

TiO_{2-x}/Ag_3PO_4 photocatalyst: oxygen vacancy dependent visible light photocatalytic performance and BPA degradative pathway, Maters. Sci. Semicond. Proc. 97 (2019) 1–10.
[68] L.H. Wang, J. Jiang, S.Y. Pang, Y. Zhou, J. Li, S.F. Sun, Y. Gao, C.C. Jiang, Oxidation of bisphenol A by nonradical activation of peroxymonosulfate in the presence of amorphous manganese dioxide, Chem. Eng. J. 352 (2018) 1004–1013.
[69] X.J. Yang, X.M. Xu, X.C. Xu, J. Xu, H.L. Wang, R. Semiat, Y.F. Han, Modeling and kinetics study of Bisphenol A (BPA) degradation over an $FeOCl/SiO_2$ Fenton-like catalyst, Catal. Today 276 (2016) 85–96.
[70] M. Molkenthin, T. Olmez-Hanci, M.R. Jekel, I. Arslan-Alaton, Photo-Fenton-like treatment of BPA: effect of UV light source and water matrix on toxicity and transformation products, Water Res. 47 (2013) 5052–5064.
[71] J. Sharma, I.M. Mishra, V. Kumar, Mechanistic study of photo-oxidation of Bisphenol-A (BPA) with hydrogen peroxide (H_2O_2) and sodium persulfate (SPS), J. Environ. Manag. 166 (2016) 12–22.
[72] W.F. Li, R. Yu, M. Li, N. Guo, H.W. Yu, Y. Yu, Photocatalytical degradation of diclofenac by Ag-BiOI-rGO: kinetics, mechanisms and pathways, Chemosphere 218 (2019) 966–973.
[73] X. Xiao, R. Hao, M. Liang, X.X. Zuo, J.M. Nan, L.S. Li, W.D. Zhang, One-pot solvothermal synthesis of three-dimensional (3D) BiOI/BiOCl composites with enhanced visible-light photocatalytic activities for the degradation of bisphenol-A, J. Hazard. Maters. 233 (2012) 122–130.
[74] L.L. Zhou, Y.Z. Dai, J. Guo, R.Z. Chen, Y.C. Xie, W. Luo, Novel $Ag_3PO_4/LaCo_{((1-x))}BixO_{(3)}$ composite photocatalyst with enhanced photocatalytic degradation of BPA under visible light, Maters. Lett. 213 (2018) 387–390.
[75] N.S. Hassan, A.A. Jalil, N.F. Khusnun, M.W. Ali, S. Haron, Role of reduced graphene oxide in improving interfacial charge transfer of hybridized rGO/silica/zirconia for enhanced Bisphenol a photodegradation, J. Alloy. Compd. 789 (2019) 221–230.
[76] J.X. Lv, X.M. Liu, P.C. Li, W. Jin, J. Xu, Y.P. Zhao, AgI loading BiOI composites with enhanced photodegradation efficiency for bisphenol A under simulated solar light, Sci. Total Environ. 669 (2019) 194–204.
[77] S.Y. Qu, Y.H. Xiong, J. Zhang, Fabrication of GO/CDots/BiOI nanocomposites with enhanced photocatalytic 4-chlorophenol degradation and mechanism insight, Sep. Purif. Technol. 210 (2019) 382–389.
[78] L. Yang, C. Xu, F.C. Wan, H.H. He, H.S. Gu, J. Xiong, Synthesis of RGO/BiOI/ZnO composites with efficient photocatalytic reduction of aqueous Cr(VI) under visible-light irradiation, Maters. Res. Bull. 112 (2019) 154–158.